85th Steelmaking Conference, (Mar.10-13, 2002, Nashville, TN), Vol.85, ISS, Warrendale, PA, 2002, pp463-476

NUCLEATION AND GROWTH OF ALUMINA INCLUSIONS DURING STEEL DEOXIDATION

Dr. Lifeng ZHANG
Dept. of Mechanical Engineering, University of Illinois at Urbana-Champaign
140 Mech. Engg. Buldg., 1206 W. Green St., Urbana, IL 61801, USA
Tel: 217-244-4656 Fax: 217-244-6534 Email: zhang25@uiuc.edu

Prof. Wolfgang Pluschkell
Institut für Metallurgie, Technical University of Clausthal,
Robert-Koch-Str.42, D-38679, Clausthal-Zellerfeld, Germany

Prof. Brian G. Thomas
Dept. of Mechanical Engineering, University of Illinois at Urbana-Champaign
140 Mech. Engg. Buldg., 1206 W. Green St., Urbana, IL 61801, USA
Tel: 217-333-6919 Fax: 217-244-6534 Email: bgthomas@uiuc.edu

Key words: Alumina, Inclusion, Nucleation, Growth, Brownian Collision, Turbulent Collision, Ostwald-ripening, Size Distribution

INTRODUCTION

It is well known that nonmetallic inclusions significantly degrade the mechanical properties of steel. The inclusion evolution process is shown in **figure 1**: ① Shortly after adding deoxidizer, particles nucleate, precipitate, and quickly grow. This stage is mainly controlled by diffusion of the deoxidization elements and oxygen [1-6]. "Ostwald-ripening"[1, 2, 6-8] occurs when the different molecular diffusion and dissociation rates due to inclusion size causes larger particles to grow at the expense of causing smaller particles to shrink. This is because of the different surface tension and oxygen concentration gradients near particles of different size. [7], Brownian motion is another cause of collisions [1-4, 6]; ② After particles grow large enough, turbulent collision [1-3, 7] and Stokes collision [2, 4, 6-8] control their continued growth; ③ Due to the density difference between

liquid steel and inclusions, bubble attachment, and fluid transport in the metallurgical vessel, larger inclusions are removed; ④ Small inclusions stay suspended in the liquid steel and are passed on to the next process while other are removed by the top slag and refractory walls by diffusion deoxidation and interfacial reactions. *Quantitative evaluation of these mechanisms should be investigated.*

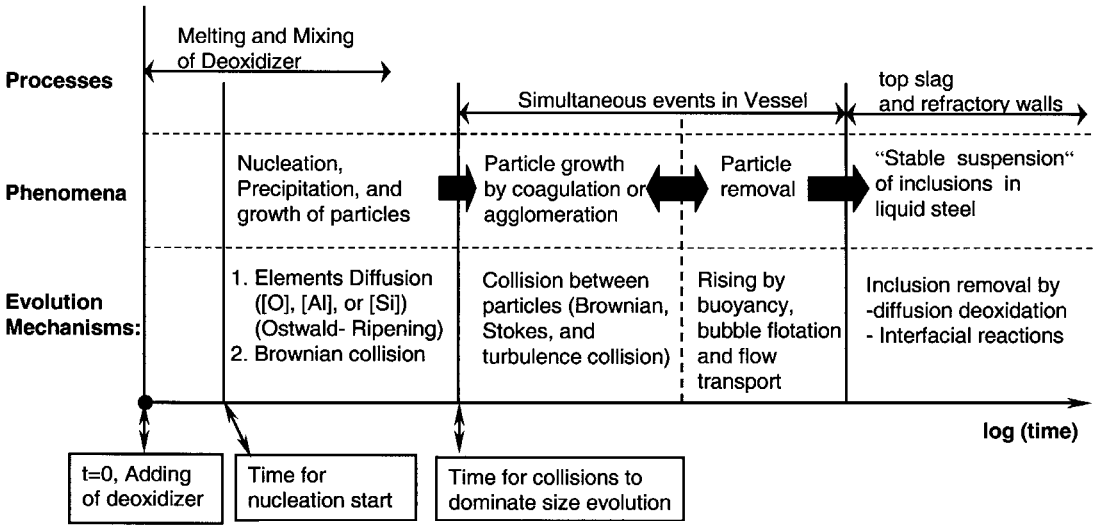

Fig.1 Inclusion evolution mechanism in liquid

The indigenous inclusions observed in low-carbon aluminum-killed steel take many forms, such as clusters of dendritic alumina (30 to 100μm size **figure 2a** [9]) and coral-shaped alumina (<50μm in size, **figure 2b**[9]). Their common characteristic [1, 9-21]: of the central globule, second arms, or the separate spherical inclusions in these clusters is their size is consistently 1~4 μm (**Fig.2c**). *The reason for this should be investigated.*

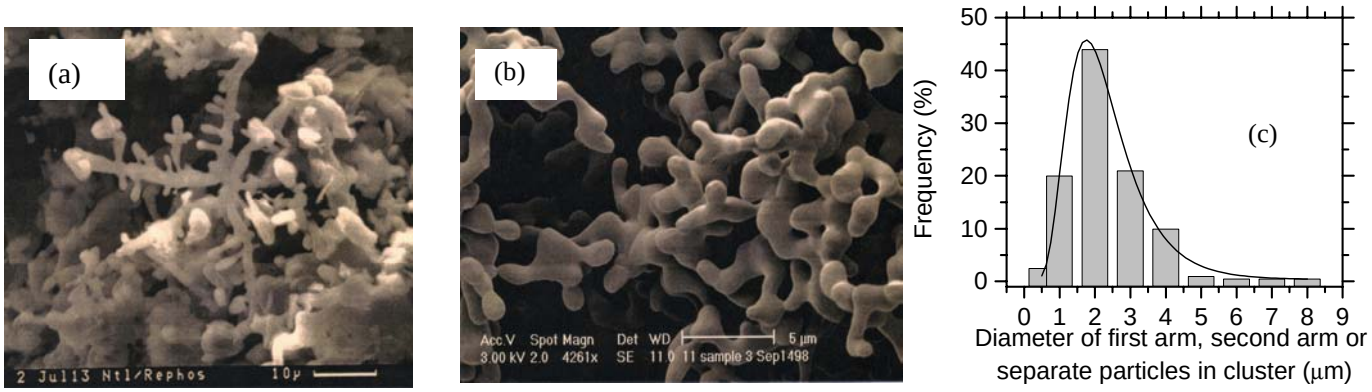

Fig.2 Alumina inclusion morphologies: a) dendritic cluster, b) coral structure and c) the diameter distribution of the globe center, secondary arms or separate spherical particles in alumina clusters

The decrease in mechanical properties of steel depends not only on the amount, composition, and morphology of inclusions but also on their size and number distribution. Inclusion size distributions have been reported from three-dimensional experimental measurements [2, 22] on samples from ladles and tundishs [23]. During deoxidation, the total number of particles large than 3μm in diameter is around 10^6-10^7 per kg at 0.5 and

1.5 min after aluminum addition [1-3]. Several researchers have modeled inclusion growth in liquid steel by collision and coagulation [21, 23, 24] However, the initial inclusion size distributions employed in these researches all used measurements for their initial conditions. *The formation and evolution of the initial size distribution should be investigated.*

This paper investigates the nucleation and growth of inclusions, focusing on the initial stages. The thermodynamic fundamentals of nucleation and precipitation are first discussed. Then a computational model for nucleation and growth of inclusions is developed and applied to simulate isothermal ladle deoxidation of steel with aluminum. The contribution of the different growth mechanisms on alumina inclusion nucleation and growth is studied. The start and evolution of inclusion size distribution with time are numerically investigated.

THERMODYNAMIC FUNDAMENTALS OF NUCLEATION

The process of nucleation of primary inclusions by the addition of deoxidizer to an oxygen-containing melt is governed by the following reaction:

$$n[\mathrm{Me}] + m[\mathrm{O}] \Leftrightarrow (\mathrm{Me}_n\mathrm{O}_m)\,. \tag{1}$$

According to classical homogenous nucleation theory, the second phase (products) start to form from the parent phase (reactants) when the change in Gibbs' free energy, ΔG, is zero:

$$\frac{d\Delta G}{dr} = 0\,. \tag{2}$$

For spherical particles, the volume free energy released must balance the surface energy created, as follows:

$$\Delta G = \frac{4}{3}\pi r^3 \Delta G_V + 4\pi r^2 \sigma\,. \tag{3}$$

The change of the free energy per unit volume ΔG_V is represented by

$$\Delta G_V = -\frac{RT}{V_m}\ln\Pi\,, \tag{4}$$

where the supersaturaion, Π, is the ratio of the actual and equilibrium concentrations:

$$\Pi \equiv \frac{C_t}{C_{eq}}\,. \tag{5}$$

Because $a_{\mathrm{Me}n\mathrm{O}m}$=1 when the deoxidation product is very pure,

$$C_t / C_{eq} = K / K_e = (\%\mathrm{Me})^n (\%\mathrm{O})^m / K_e\,. \tag{6}$$

Solving Eq.(2) and Eq.(3) gives

$$\Delta G_V = -\frac{2\sigma}{r_C}\,. \tag{7}$$

Coupling Eq.(4), (5) and (7) yields the critical radius of nucleus r_C to be

$$r_C \equiv \frac{2\sigma V_m}{RT\ln\Pi}\,. \tag{8}$$

If $r > r_C$, nucleation occurs, and stable particles precipitate and start to grow. According to Eq.(8), the critical size of nucleus decreases with increasing supersaturaion and decreasing surface tension. Because supersaturaion evolves with time during the deoxidation process, the critical nucleus size also evolves with time.

NUCLEATION AND GROWTH MODEL FORMULATION

The current computational model of nucleation and growth of alumina inclusions during steel deoxidation is based on the following assumptions.

① The Gibbs-Thomson equation [25] holds for all size particles; [26]

② The basic unit of the model is the "pseudo-molecule", which consists of 5 atoms roughly arranged as Al_2O_3, which are unstable unless part of a large group. Before nucleation, groups of pseudo-molecules form by random diffusion together of single pseudo-molecules (namely the diffusion of dissolved oxygen and dissolved aluminum atoms). This assumption is also employed by Wanibe et al [27] to study the formation of the dendritic alumina clusters. If enough pseudo-molecules gather to form a stable nucleus, then nucleation (precipitation) occurs, meaning that the particle is stable and can grow by both continued diffusion of pseudo-molecules, and by collision with other stable inclusions (via Brownian collision and turbulent collision).

③ Ostwald-Ripening is considered. By this mechanism, pseudo-molecules dissolve from smaller inclusions and diffuse to and precipitate onto some larger inclusions;

④ The system is isothermal, i.e., the heat of the reaction $(i)+(j)\rightarrow(i+j)$ is neglected;

⑤ The inclusions and pseudo-molecules are spherical;

⑥ The interfacial tension is independent of size;

⑦ The simple inclusion removal model is that all inclusions with radii larger than 36μm are considered to be instantly removed to the top slag.

⑧ The effect of carbon and other alloys in the steel are ignored.

Population Balance Equations

When the aluminum is first added to the steel, pseudo-molecules will quickly form, resulting in supersaturation, Π, until they are able to diffuse and combine into larger groups:

$$\Pi \equiv \frac{N_1}{N_{1,eq}} = N_1^* = N_s^* - \sum_{i=2}^{\infty} N_i^* \cdot i \,. \qquad (9)$$

Here, Π is defined as the ratio between the number density of free pseudo-molecules (Al_2O_3 molecules) at time *t* and that at equilibrium, so is different from K/K_e in Eq.(6).

The nucleation and growth of inclusions in liquid steel is dominated by the diffusion of pseudo-molecules and collisions of particles of different size ranges. Therefore, the time evolution of the pseudo-particle group size distribution, N_i is governed by the following particle number balance relations:

① $2 < i < i_C$ (before nucleation)

$$\frac{dN_i}{dt} = -N_i\beta_{1i}N_1 + \beta_{1,i-1}N_1N_{i-1} + \alpha_{i+1}A_{i+1}N_{i+1} - \alpha_i A_i N_i \tag{10}$$

② $i \geq i_C$ (stable inclusion particles)

$$\frac{dN_i}{dt} = \underbrace{-\phi N_i \sum_{j=1}^{\infty}\delta_{ij}N_j}_{i} + \frac{1}{2}\phi\sum_{j=1}^{i-1}\delta_{j,i-j}N_jN_{i-j} \quad \text{Collision of particles}$$
$$\underbrace{-N_i\beta_{1i}N_1 + \beta_{1,i-1}N_1N_{i-1} + \alpha_{i+1}A_{i+1}N_{i+1} - \alpha_i A_i N_i}_{\text{Difussion of Molecules to } i \text{ and dissolution of molecules from } i} \tag{11}$$

Critical radius of molecular group- According to assumption ⑤, the radius of a pseudo-molecule is

$$r_1 = \left(3V_m/4\pi N_A\right)^{1/3}. \tag{12}$$

The radius of group i r_i can be expressed in terms of the number of pseudo-molecules which make up the molecular group (assumption ②):

$$r_i = r_1 i^{1/3}\ . \tag{13}$$

The critical number of pseudo-molecules needed to make a stable particle which can grow is $i=i_c$, with corresponding particle radius of r_c, which is found from Eq.(8)(12)(13) by:

$$i_C = \frac{32\pi}{3}V_m^2N_A\left(\frac{\sigma}{RT}\right)^3\left(\frac{1}{\ln\Pi}\right)^3. \tag{14}$$

Rate constant of pseudo-molecule diffusion, β_{1i}— Assuming a uniform psuedo-molecule concentration field with a boundary layer thickness of r_i, the diffusion rate of single molecules to form a molecular groups containing i pseudo-molecules (either subcritical or stable particles) is expressed by [26]

$$\beta_{1i} = 4\pi D_1 r_i. \tag{15}$$

Rate Constant of particle diffusion, δ_{ij}— Collision is considered only between stable particles, according to a rate constant that includes two components:

$$\delta_{ij} = \frac{2kT}{3\mu}\left(1/r_i + 1/r_j\right)\left(r_i + r_j\right) + 1.3\left(r_i + r_j\right)^3\left(\varepsilon/\nu\right)^{1/2} \tag{16}$$

The first term represents Brownian collision [28] and the second term represents turbulent collision, based on Saffman's model [29].

Dissolution rate, α_i — Ostwald-ripening involves both growth (from diffusion governed by β_{1i}) and dissociation, which is governed by α_i, which is found by tracking the diffusion of pseudo-molecules, β_{1i}, where i is the number of pseudo-molecules in each inclusions. Unstable particles, ($i<i_c$) can grow or shrink only due to diffusion, while stable inclusion particles, ($i>i_c$ and $r>r_c$) evolve according to both diffusion and collision.

Solution Algorithm

Eqs.(9)-(11) are solved using the Runge-Kutta method. As an initial condition, the N^*_s is taken as a function of dimensionless time, based on the study of Kampmann and Kahlweit which assumes that the pseudo-molecules are produced within the system by an isothermal first order reaction,

$$N_s^*(t^*) = N_{s,eq}^* \left[1.0 - \exp(-Bt^*)\right], \tag{17}$$

where $N^*_{s,eq}N_{1,eq}$ is the final number of pseudo-molecules produced by the reaction.

Initially, there are no other size groups in the system a:

$$N^*_i(t^*=0)=0 \qquad i>1 \tag{18}$$

The following parameters are chosen to model steel deoxidation with these equations: V_m= 34.4×10^{-6} m^3/mol [30], T=1873K, $N^*_{s,eq}$=100. and B=0.1 [26], D_1=3.0×10^{-9} m^2/s (diffusion coefficient of oxygen in liquid steel) [31], $N_{1,eq}$=2.634×10^{23} m^{-3} m^{-3} corresponding to the 3ppm dissolved oxygen in steel, ρ_L=7000 kg/m^3, ρ_p =2700 kg/m^3, μ_L=0.0067 kg.m^{-1}s^{-1}. The surface tension between Al_2O_3 particle and liquid steel is 2.3N/m at this temperature [32] However, this value changes greatly with oxygen content and particle size [33], so 0.5 N/m is assumed for σ here, according to Wasai et al [33]. Therefore, r_1=2.39× 10^{-10} m (Eq.(8)), $\beta_{11} \approx 9.0\times10^{-18}$ m^3/s (Eq.(15)), $t^* \approx 2.371\times10^6 t$.

.

RESULTS OF NUMERICAL SIMULATION

The model was applied to aluminum deoxidation of a typical steel-oxygen system, where measurements and calculations were available. The vessel was a 50 tonne ladle of low-carbon steel refined in an ASEA-SKF furnace. The total oxygen before adding aluminum is around 300 ppm and the final free oxygen is about 3 ppm, (which corresponds to a 46kg aluminum addition). The ladle had 2.3m diameter and 1.7m depth, which corresponds to a turbulent energy dissipation rate in the melt of 0.01224 m^2/s^3 (856.8 erg/cm^{3}s).

Control Mechanisms of Inclusion Growth at Different Inclusion Size Ranges

A comparison of the pseudo-molecules diffusion rate constant β_{1i} with different collision rate constants δ_{ij} is shown in **figure 3**. It can be concluded that ① When r<1μm, the particle growth is dominated by diffusion of pseudo-molecules (Ostwald-Ripening) and Brownian collision of particles. The contribution of Brownian collision to accelerate the growth of larger inclusions is very clear from **figure 4**. The irregular thermal movement that characterizes Brownian collisions is independent of fluid flow, and is not directional. Thus the inclusions tend to grow in every direction, leading to a spherical product. ② When r>2μm, particle growth is dominated by the turbulent collision of particles. During this stage, the diffusion of pseudo-molecules is not as important, due to the low concentration of pseudo-molecules. The process of Ostwald-ripening continues to act by smoothing the irregular morphology of inclusion dendrite or cluster surfaces by dissolving Al_2O_3 molecules from regions of high curvature (eg. small particles) and diffusing to the flatter surfaces, (such as found on large

particles). However, during this stage, turbulent collisions dominate particle growth, so the inclusion morphology tends to become more jagged and it can retain a cluster shape. Thus, 1~2μm is a size threshold where the growth mechanism of inclusions changes from the diffusion of pseudo-molecules (Ostwald ripening) and Brownian collision to turbulent collision. This explains why the smallest features of real inclusion clusters are about this size.

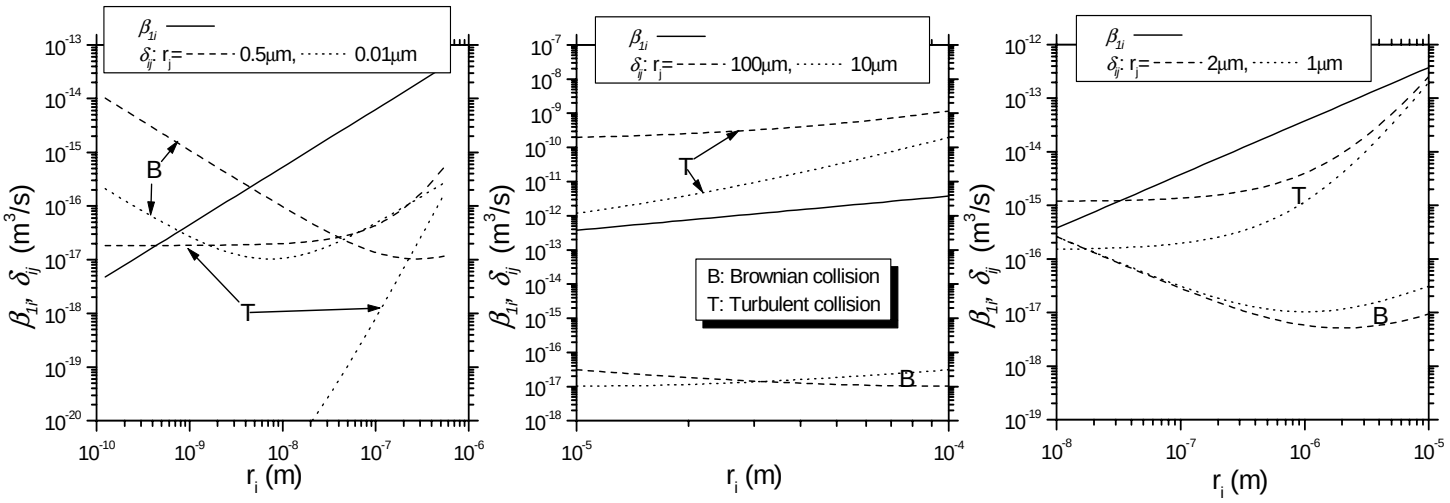

Fig.3 Comparison of pseudo-molecule diffusion rate constant β_{1i} and collision rate constants δ_{ij}.

The following scales can be defined:

- Brownian scale l_B<1μm; where the growth of inclusions with radii in this range is controlled by diffusion of pseudo-molecules and Brownian collision. Solid inclusions in this range tend to be spherical;
- Turbulent scale l_T=2~l_e, where l_e is the characteristic size of the smallest turbulence eddy, on the order of $l_e=(\nu^3/\varepsilon)^{1/4}$, which is around 90μm for the current system. Inclusions with radii in this range grow by turbulent collisions, and solid inclusions in this range tend to retain smallest features of 1~4μm in diameter as shown in Fig.2;
- Intermediate scale $l_I=l_B$~l_T, where the growth of inclusions in is controlled both by pseudo-molecules diffusion and by collisions (Brownian collision and turbulent collision);
- Macro scale $l_M>l_e$. where the effect of inclusion buoyancy on its motion through the fluid cannot be neglected.

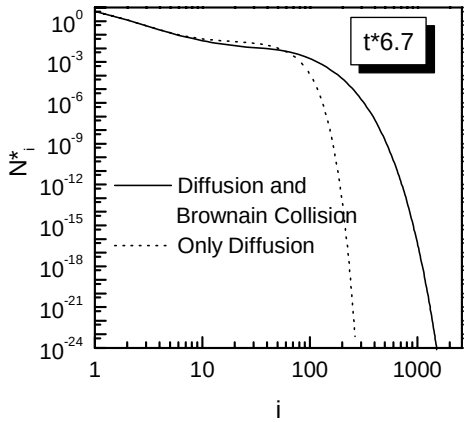

Fig.4 Contribution of Brownian collision of precipitated inclusions on the growth of inclusions

Inclusion morphology is therefore summarized as follows: Fine inclusions grow spherically to 1 to 2 μm in radii due to diffusion and Brownian collision after nucleation. When there is a shortage of nuclei, single particles can grow into large dendritic structures due to unstable growth into high concentrations of diffusing pseudo-molecules. Otherwise, clusters of particles will form due to turbulent collisions resulting from flowing

liquid steel. With time, the surface contours of all particles become progressively smoother due to "Ostwald ripening".

Incubation, Nucleation and Growth of Inclusions

Figure 5 shows the supersaturation Π , the number of particles ζ and the critical size of nucleus i_c as a function of time. **Table I** summarizes some calculation results.

Incubation period- Before aluminum is added into the liquid steel, only dissolved oxygen is present in the melt. There are no pseudo-molecules, nucleii or inclusions. After aluminum addition, the aluminum and oxygen react to form pseudo-molecules. Groups of pseudo-molecules are generated from diffusion. With the further addition and dispersion of aluminum, the concentration of pseudo-molecules continues to increase. After Π=1 (t=t_1), with further increasing of Π, the critical radius r_c decreases (Eq.(8)). Numerical calculations show that t^*_1=0.1 (t_1=0.042μs). At the critical time, t=t_2, the radii of some groups of pseudo-molecules become equal to r_c, thus nucleation begins. Particles precipitate and start to grow. Thus the incubation period is 0~t_2. When t<t_2, ζ=0. Fig.5 and Table I show t^*_2=1.25 (t_2=0.53μs). Thus, the incubation period is very short, only 0.53μs. At t=t_2, the first particle appearing in the melt has i_c=42 (r=8.3 Å), which means that a group of 42 pseudo-molecules must form by a random fluctuation.

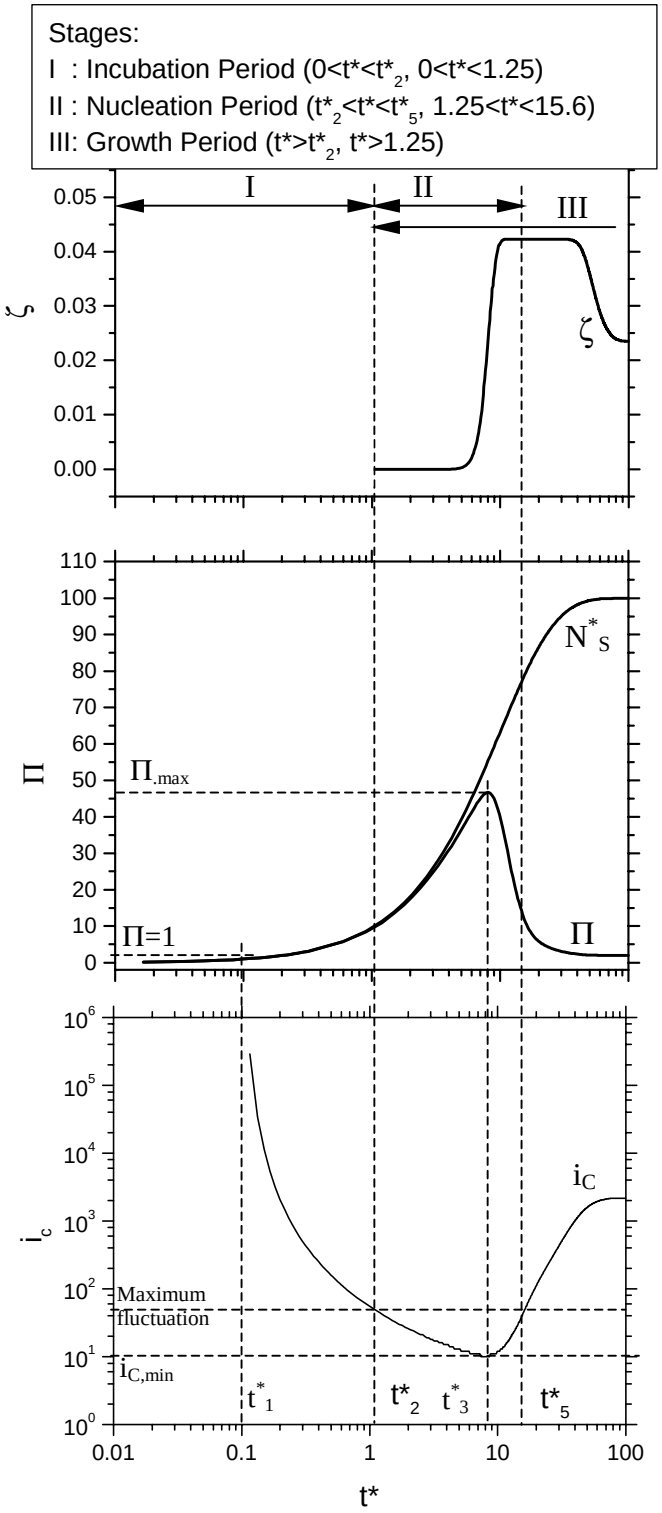

Fig.5 Calculated ζ, Π, i_c *versus* time

Nucleation period- A maximum concentration of pseudo-molecules develops for a given aluminum addition and distribution. The supersaturation Π gradually increases from zero to its maximum (46.7) at time t^*_3 =8.07 (t_3=3.40μs). This corresponds to the decrease in critical nucleus size to its smallest-sized stable nucleus (r_c =5.15Å, containing i=10 pseudo-molecules) at time t_3 (Eq.(8)). Groups containing less than 10 pseudo-molecules are not stable particles.

Because pseudo-molecules are continuously consumed by growing particles, the supersaturation decreases slowly after this time t_3, as r_c steadily increases (Eq.(8)).

Nucleation is possible only during the time period t^*_2~t^*_5 (0.53~6.58μs), when the critical nucleus size is smaller than the largest sized group of pseudo-molecules (forming by random diffusion). This agrees with the study of Kawawa et al [4], which reported the deoxidizing reaction is complete almost immediately after the deoxidizer is transported to a given location in the melt.

After time t^*_5=15.6, (t_5=6.58μs), no new particles can nucleate. The supersaturation is asymptotic to 1 (equilibrium) as time approaches infinity. Stable particles remaining in the melt continue to grow by diffusion of pseudo-molecules and collision with other inclusions, or dissolve by Ostwald-Ripening. Thus, the total number of particles gradually decreases after t_5.

Table I Computed results at critical times

	t^*	t (μs)	Π	i_C	i_S	ζ
t^*_1	0.1	0.042	1.0	∞	0	0
t^*_2	1.25	0.53	12.4	42	42	4.56×10^{-24}
t^*_3	8.07	3.40	43.6	10	10	5.2×10^{-3}
t^*_5	15.6	6.58	11.4	42	10	4.23×10^{-2}
$>t^*_5$	>15.6	>6.58	↓	↗	10	↓

The nucleation rate at maximum supersaturation is 1.54×10^{-2} (5.02×10^{27} m^{-3} s^{-1}). Kahlweit et al recommended an analytical expression [26], which yields a maximum nucleation rate of 5.80×10^{-7} for the current system. This is partly because the analytical solution includes only diffusion of pseudo-molecules while the current numerical simulation also considers collisions. However, this huge discrepancy needs further investigation.

Growth period- Figure 6 shows a histogram of inclusion size distribution at different times. As previously discussed, at time 0.53μs (t_2), the first size inclusions with radii of 8.31Å nucleate and precipitate. At this time, only one size exists. After time t_2, smaller inclusions can precipitate and grow by diffusion of pseudo-molecules, and collision with other inclusions. This starts a size distribution range. With increasing time, this size distribution range becomes larger and larger. Thus, size distribution expressed as a function of time after the addition of deoxidizer contributes to the precipitation, collision/coagulation and flotation of inclusions. On the other hand, with increasing time, the number density of smaller inclusions decreases while and that of the larger ones increases, due to both Ostwald-Ripening and collision. In addition to smoothening the alumina surface roughness, Ostwald-ripening leads to the evolution of inclusion size distribution. When t=6s, the largest inclusion is around 2 μm diameter. According to the industrial measurements [34], the largest inclusion diameter, after 6 s second deoxidation, was around 2-5 μm, which agrees roughly with current calculation. Fig.6 also indicates that when the inclusion size is in the turbulent scale range, growth is controlled mainly by the turbulent collisions. This expands the range of the size distribution from 0.1~1μm at 6s to 0.1~36μm at 100s.

Figure 7 indicates that with increasing time, the number of smaller inclusions drops, and some new bigger inclusions are generated mainly by collision. The inclusion concentration changes with time: first increasing to a maximum value and then slowly decreasing. It takes about 100sec for the inclusions growth into several tens of microns, which agreeswell with the study of Kawawa et al [4]. **Figure 8** compares the total oxygen content between the current calculation and an experiment by Nakanishi [35], which shows rough agreement. After 720 seconds (12min), the total oxygen concentration in the liquid decreases to around 20 ppm.

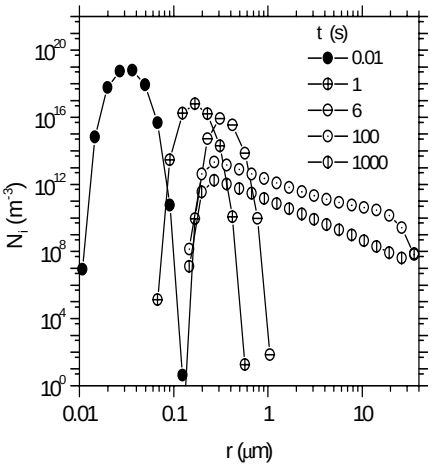

Fig.6 Inclusion size distribution as a function of time

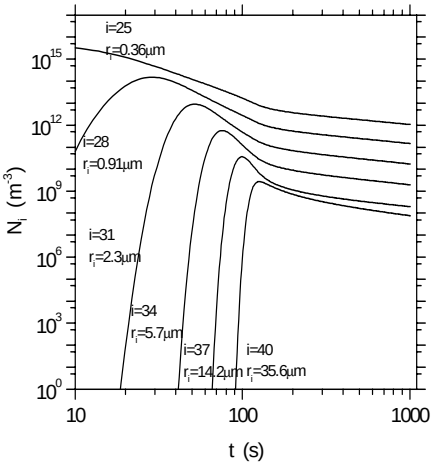

Fig.7 Inclusion concentration *versus* time

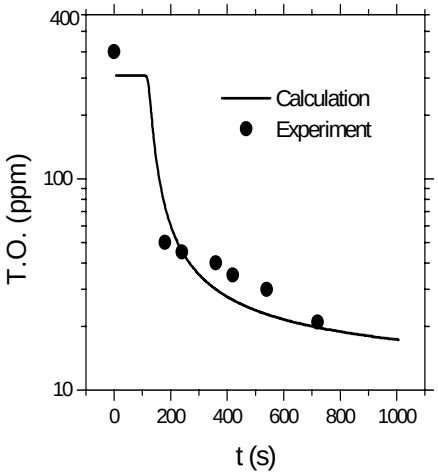

Fig.8 Comparison of total oxygen between calculation and experiment

CONCLUSIONS AND SUMMARY

1. A computational model based on classic homogenous nucleation theory, thermodynamic analysis and numerical simulation, has been developed to study steel deoxidation by aluminum in a low carbon aluminum-killed steel ladle. The model calculates the nucleation and time evolution of the alumina inclusion size distribution due to Ostwald ripening, Brownian collision and turbulent collision.

2. For the given conditions, (which assume that the pseudo-molecules of Al_2O_3 all appear within about 50 μs), the nucleation is very fast, occurring mainly between 1μs and 10μs. The stable inclusion nuclei are predicted to be only about 10-20 Å in diameter (containing on the order of 10-100 pseudo-molecules of alumina). After this time, the size distribution of the stable inclusion particles grows by diffusion of pseudo-molecules (Ostwald-Ripening) and by collisions. Thus, deoxidation proceeds rapidly.

3. Ostwald-ripening due to the diffusion of pseudo-molecules helps nuclei to appear and grow, causes smaller inclusions to dissolve, continues to precipitate pseudo-molecules onto growing large inclusions, and tends to smoothen the rough surfaces of dendritic or cluster inclusions.

4. The growth of inclusions smaller than 1μm, is mainly controlled by diffusion of pseudo-molecules and Brownian collision. Inclusions in this range tend to be spherical. The growth of inclusions larger than 2μm is mainly controlled by turbulent collisions. Inclusions in this range tend to form clusters which retain minimum

feature sizes of 1~2μm.

5. When inclusion size increases and turbulent collisions dominate their growth, the size distribution greatly extends, creating macroinclusions that can be removed by buoyancy. Computations of the inclusion size range including these phenomena roughly agree with experimental measurements.

6. Further studies should include the effect of deoxidant composition (Si and Al), deoxidant flow transport, interfacial tension, diffusion coefficient, the initial oxygen content, and temperature on inclusion nucleation and growth. In addition, the phenomena of bubble-related collisions, cluster morphology, reoxidation, realistic inclusion transport in the flowing liquid, and removal at the top slag layer and walls on inclusion evolution also need investigation before steel deoxidation and inclusion formation processes can be fully understood.

NOMENCLATURE

A_i	The surface area of particle i, m^2
B	The rate constant in Eq.(19)
C_{eq}	The saturation concentration in equilibrium with a plane interface of the new phase, or the concentration of solute in the parents phase when r is infinite, m^{-3}
C_t	The average concentration of the precipitating substance (solute), m^{-3}
D_1	the diffusion coefficient of the pseudo-molecules in liquid , m^2s^{-1}
ΔG	The change of the Gibbs' free energy, J
ΔG_V	The change of the free energy per unit volume, Jm^{-3}
i, j	The particle size, namely, this particle is comprised of i pseudo-molecules or j pseudo-molecules
i_c	the critical size for nucleus
i_S	The smallest particle size
j_{stat}	The dimensionless stationary nucleation rate
K	and or the concentration product at an arbitrary moment after deoxidation Eq.(6)
K_e	the thermodynamic solubility product, namely, the equilibrium constant
k	The Boltzmann constant, $J.K^{-1}$
N_A	The Avogadro number, mol^{-1}
N_1	The concentration of the dissolved pseudo-molecules, m^{-3}
$N_{1,eq}$	The concentration of the dissolved pseudo-molecules at equilibrium, m^{-3}
N_i	The average concentration of the particle i, m^{-3}
N^*_i	The dimensionless number density of particle i
$N^*_s(t^*)$	The total dimensionless number density of pseudo-molecules including those in the particles
R	The gas constant, 8.314 $J.K^{-1}mol^{-1}$
r	The particle radius, m
r_c	The critical radius for nucleation, m
r_i	The radii of the particle i , m
r_1	the radius of the pseudo-molecule, m
T	The absolute temperature, K
t	Time, s
t_1	Time at $\Pi=1$, s
t_2	Time for the beginning of nucleation, s
t_3	Time at $\Pi=\Pi_{max}$, s

t_5 Time for the ending of nucleation period, s
t^* The dimensionless time
V_m the molar volume, $m^3 mol^{-1}$
α_i The number of pseudo-molecules which dissociate per unit time from unit area of a particle of class i, $m^{-2} s^{-1}$
β_{1i} The rate constant of the growth reaction $(i)+(1) \rightarrow (i+1)$, $m^3 s^{-1}$
δ_{ij} Collison rate constant, m^3/s
ε The turbulent energy dissipation rate, $m^2 s^{-3}$
Π The supersaturaion of the parents phase, or the dimensionless concentration of pseudo-molecules
Π_{max} The maximum supersaturation
μ The viscosity of the liquid, $kg.m^{-1} s^{-1}$
ϕ The inclusion oagulation coefficient [36]
ρ_L The density of liquid, $kg.m^{-3}$
ρ_p The density of particles, $kg.m^{-3}$
σ The interfacial tension between alumina and liquid steel, $N.m^{-1}$
ζ The total dimensionless number density of growing particles
ν The viscosity of the liquid, $m^2 s^{-1}$

REFERENCES

1. E.T. Turkdogan, "Deoxidation of Steel," JISI, 1972, 21-36.
2. Y. Miyashita and K. Nishikawa, "Measurement of Size Distribution of Nonmetallic Inclusions in Steel," Trans. ISIJ, Vol. 8, 1968, 181-185.
3. S. Linder, "Hydrodynamics and Collisions of Small Particles in a Turbulence Metallic Melt with Special Reference to Deoxidation of Steel," Scand. J. Metallurgy, Vol. 3, 1974, 137-150.
4. T. Kawawa and M. Ohkubo, "A Kinetics on Deoxidation of Steel," Trans. ISIJ, Vol. 8, 1968, 203-219.
5. E.T. Turkdogan, "Nucleation, Growth, and Flotation of Oxide Inclusions in Liquid Steel," JISI, 1966, 914-919.
6. M. Suzuki, R. Yamaguchi, K. Murakami, M. Nakada, "Inclusion Particle Growth during Solidification of Stainless Steel," ISIJ Inter., Vol. 41 (3), 2001, 247-256.
7. U. Lindborg and K. Torssell, "A Collision Model for the Growth and Separation of Deoxidation Products," Trans. ASME, Vol. 242, 1968, 94-102.
8. K. Nogi, "Wetting Phenomena in Materials Processing," Tetsu-to-Hagane, Vol. 84 (1), 1998, 1-6.
9. R. Rastogi and A.W. Cramb, "Inclusion Formation and Agglomeration in Aluminum-killed Steels," in 2001 Steelmaking Conference Proceedings, Vol. 84, ISS, Warrendale, (Baltimore, Maryland, USA), 2001, 789-829.
10. R.A. Rege, E.S. Szekeres and W.D. Forgeng, "Three-Dimensional View of Alumina Clusters in Aluminum-Killed Low-Carbon Steel," Met. Trans. AIME, Vol. 1 (9), 1970, 2652.
11. K. Okohira, N. Sato and H. Mori, "Observation of Three-Dimensional Shapes of Inclusions in Low-Carbon Aluminum-Killed Steel by Scanning Electron Microscope," Trans. ISIJ, Vol. 14, 1974, 103-109.

12. M. Olette, "Institut de Recherches de La Siderurgie Francaise," Report, IRSIO, 1972.
13. K. Asano and T. Nakano, "Deoxidation of Molten Steel with Deoxidizer," Trans. ISIJ, Vol. 12, 1972, 343-349.
14. H. Ooi, T. Sekine and G. Kasai, "On the Mechanisms of Alunima Cluster Formation in Molten Iron," Trans. ISIJ, Vol. 15, 1975, 371-379.
15. N. Aritomi and K. Gunji, "Morphology and Formation Mechanism of Dendritic Inclusions in Iron and Iron-Nickel Alloys Deoxidized with Silicon and Solidified Unidirectionally," Trans. ISIJ, Vol. 19, 1979, 152-161.
16. T.B. Braun, J.F. Elliott and M.C. Flemings, "The Clustering of Alumina Inclusions," Metal. Trans. B, Vol. 10B (6), 1979, 171-184.
17. N. Aritomi and K. Gunji, "On the Formation of Dendritic Inclusion from a Spherical Primary Silica in Iron-10% Nickel Alloy Deoxidized with Silicon," Trans. ISIJ, Vol. 20, 1980, 26-32.
18. Y. Miki, H. Kitaoka, T. Sakuraya, T. Fujii, "Mechanism for Separating Inclusions from Molten Steel Stirred with a Rotating Electro-Magnetic Field," ISIJ Inter., Vol. 32 (1), 1992, 142-149.
19. W.K. Tiekink, A. Pieters and J. Hekkema, "Al2O3 in Steel: Morphology Dependent on Treatment," I & Smaker, Vol. 21 (7), 1994, 39-41.
20. T. Murai, H. Matsuno, E. Sakurai, H. Kawashima, "Separation Mechanism of Inclusion from Molten Steel during RH Treatment," Tetsu-to-Hagane, Vol. 84 (1), 1998, 13-18.
21. L. Zhang and S. Taniguchi, "Fluid Flow and Inclusion Removal in Continuous Casting Tundish," Metal. & Material Trans. B., Vol. 31B (2), 2000, 253-266.
22. A.S. Venkatadri, "Mechanism of Formation of Non-metalli Inclusions in Aluminum-killed Steel," Trans. ISIJ, Vol. 18, 1978, 591-600.
23. Y. Miki and B.G. Thomas, "Modeling of Inclusion Removal in a Tundish," Metall. Mater. Trans. B, Vol. 30B (4), 1999, 639-654.
24. Y. Miki, B.G. Thomas, A. Denissov, Y. Shimada, "Model of Inclusion Removal During RH Degassing of Steel," Iron and Steelmaker, Vol. 24 (8), 1997, 31-38.
25. J. Miyake and M.E. Fine, "Electrical Resistivity and the Gibbs-Thomson Equations," Scripta Metallurgica et Materialia, Vol. 25, 1991, 191-194.
26. L. Kampmann and M. Kahlweit, "On the Theory of Precipitations II," Berichte der Bunsen-Gesellschaft physikalische Chemie, Vol. 74 (5), 1970, 456-462.
27. Y. Wanibe and K. Sano, J. Met. Soc., Vol. 31, 1967, 795.
28. S. Taniguchi and A. Kikuchi, "Mechanisms of Collision and Coagulation between Fine Particles in Fluid," Tetsu-to-Hagane, Vol. 78 (4), 1992, 527-535.
29. P.G. Saffman and J. S. Turner, "On the Collision of Drops in Turbulent Clouds," J. Fluid Mech., Vol. 1, 1956, 16-30.
30. K. Mukai, H. Sakao and K. Sano, "Non-metallic Inclusions Formed by Deoxidation Reaction in the Deoxidation Process- Deoxidation Reaction Zone," Trans. ISIJ, Vol. 9, 1969, 196-203.
31. K. Mori and K. Suzuki, "Diffusion of Oxygen in Liquid Iron," Trans. ISIJ, Vol. 12, 1972, 464-471.

32. M.L. Turpin and J.F. Elliott, "Nucleation of Oxide Inclusions in Iron Melts," JISI, 1966, 217-225.
33. K. Wasai and K. Mukai, "Thermodynamics of Nucleation and Supersaturation for the Aluminum-Deoxidation Reaction in Liquid Iron," Metal. & Material Trans. B., Vol. 30B (6), 1999, 1065-1074.
34. F. Oeters, Metallurgy of Steelmaking, Verlag Stahleisen mbH, 1994, 347.
35. K. Nakanishi and J. Szekely, "Deoxidation Kinetics in a Turbulent Flow Field," Trans. ISIJ, Vol. 15, 1975, 522-530.
36. T. Nakaoka, S. Taniguchi, K. Matsumoto, S.T. Johansen, "Particle-Size-Grouping Method of Inclusion Agglomeration and its Application to Water Model Experiments," ISIJ Inter., Vol. 41 (10), 2001, 1103-1111.